BIOCHEMISTRY
including biophysical chemistry & molecular biology

Article

pubs.acs.org/biochemistry



# Enzymatic and Cryoreduction EPR Studies of the Hydroxylation of Methylated $N^{\omega}$-Hydroxy-L-arginine Analogues by Nitric Oxide Synthase from *Geobacillus stearothermophilus*

Roman Davydov,[†] Kristin Jansen Labby,[†,∥] Sarah E. Chobot,[§] Dmitriy A. Lukoyanov,[†] Brian R. Crane,*[,§] Richard B. Silverman,*[,‡] and Brian M. Hoffman*[,†]

[†]Department of Chemistry, Northwestern University, 2145 Sheridan Road, Evanston, Illinois 60208-3113, United States

[‡]Department of Chemistry, Department of Molecular Biosciences, Chemistry of Life Processes Institute, Center for Molecular Innovation and Drug Discovery, Northwestern University, Evanston, Illinois 60208-3113, United States

[§]Department of Chemistry and Chemical Biology, Cornell University, Ithaca, New York 14853-1301, United States

Supporting Information

**ABSTRACT:** Nitric oxide synthase (NOS) catalyzes the conversion of L-arginine to L-citrulline and NO in a two-step process involving the intermediate $N^{\omega}$-hydroxy-L-arginine (NHA). It was shown that Cpd I is the oxygenating species for L-arginine; the hydroperoxo ferric intermediate is the reactive intermediate with NHA. Methylation of the $N^{\omega}$-OH and $N^{\omega}$-H of NHA significantly inhibits the conversion of NHA into NO and L-citrulline by mammalian NOS. Kinetic studies now show that $N^{\omega}$-methylation of NHA has a qualitatively similar effect on $H_2O_2$-dependent catalysis by bacterial gsNOS. To elucidate the effect of methylating $N^{\omega}$-hydroxy L-arginine on the properties and reactivity of the one-electron-reduced oxy-heme center of NOS, we have applied cryoreduction/annealing/EPR/ENDOR techniques. Measurements of solvent kinetic isotope effects during 160 K cryoannealing cryoreduced oxy-gsNOS/NHA confirm the hydroperoxo ferric intermediate as the catalytically active species of step two. Product analysis for cryoreduced samples with methylated NHA's, NHMA, NMOA, and NMMA, annealed to 273 K, show a correlation of yields of L-citrulline with the intensity of the **g 2.26** EPR signal of the peroxo ferric species trapped at 77 K, which converts to the reactive hydroperoxo ferric state. There is also a correlation between the yield of L-citrulline in these experiments and $k_{obs}$ for the $H_2O_2$-dependent conversion of the substrates by gsNOS. Correspondingly, no detectable amount of cyanoornithine, formed when Cpd I is the reactive species, was found in the samples. Methylation of the NHA guanidinium $N^{\omega}$-OH and $N^{\omega}$-H inhibits the second NO-producing reaction by favoring protonation of the ferric-peroxo to form unreactive conformers of the ferric-hydroperoxo state. It is suggested that this is caused by modification of the distal-pocket hydrogen-bonding network of oxy gsNOS and introduction of an ordered water molecule that facilitates delivery of the proton(s) to the one-electron-reduced oxy-heme moiety. These results illustrate how variations in the properties of the substrate can modulate the reactivity of a monooxygenase.

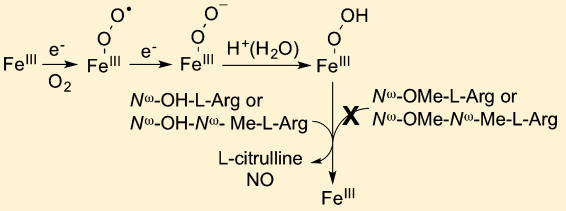


Nitric oxide synthase (NOS) catalyzes the NADPH- and $O_2$-dependent conversion of L-arginine to L-citrulline and nitric oxide (NO). NOS produces NO in two $O_2$- and NADPH-dependent monoxygenation steps; in the first step, NOS converts L-arginine into $N^{\omega}$-hydroxy-L-arginine (NHA); in the second step, NOS converts NHA to L-citrulline and NO (Scheme 1). The first step is a hydroxylation that requires delivery of two electrons to the NOS ferriheme; product formation in the second step requires only one electron overall. In both steps, $H_4B$ rapidly provides a second electron, which is necessary for oxygen activation, and the resulting $H_4B$ radical is subsequently rereduced.[1] In step one, the $H_4B$ radical is reduced by NADPH, whereas in step two, the $H_4B$ radical is presumably reduced by the initial product $NO^-$, likely via $Fe^{II}NO$.[2−4]

NO plays an essential signaling role in mammalian neurotransmission, vasodilation, and immune response[5,6] and therefore misregulation of NO production by NOS is implicated in many disease states.[7−10] NOS homologues exist in bacteria as well, including the NOS-like protein from the thermophilic bacterium *Geobacillus stearothermophilus* (gsNOS).[11,12] Most of the bacterial NOSs discovered to date, including gsNOS, are similar to mammalian $NOS_{oxy}$, but unlike mammalian NOSs, bacterial NOSs do not contain an attached reductase domain. Native reductase partners for bacterial NOSs have yet to be identified, but $H_2O_2$ is a viable *in vitro* cosubstrate.[12] When bacterial NOSs are provided a mammalian reductase domain partner and $H_4B$,[13] or if they have a fused reductase domain,[14] they can catalyze $O_2$- and NADPH-dependent oxidation of L-arginine to L-citrulline and NO. Crystal structures of bacterial NOSs show a highly conserved active site like that of mammalian NOSs, with the exception of

**Received:** April 23, 2014
**Revised:** August 28, 2014
**Published:** September 24, 2014

   dx.doi.org/10.1021/bi500485z | *Biochemistry* 2014, 53, 6511−6519

**Scheme 1. Reaction Catalyzed by NOS**

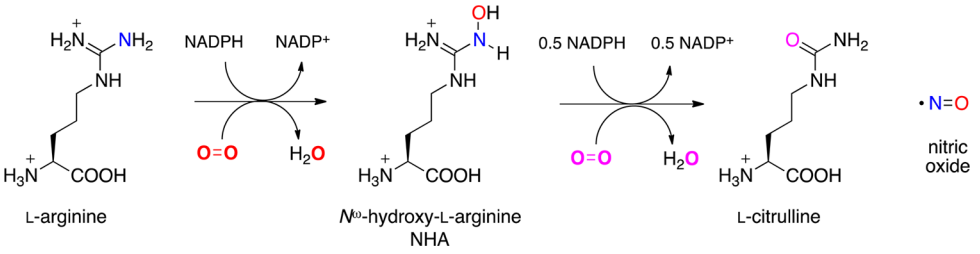


minor changes just outside the active site that likely contribute to gsNOS's enhanced stability.[11,15]

The NOS monooxygenation reactions occur via heme-catalyzed reductive $O_2$ activation similar to the cytochromes P450 (Scheme 2). This sequence of reactions begins with

**Scheme 2. Heme-Oxy Species Formed during Catalysis**

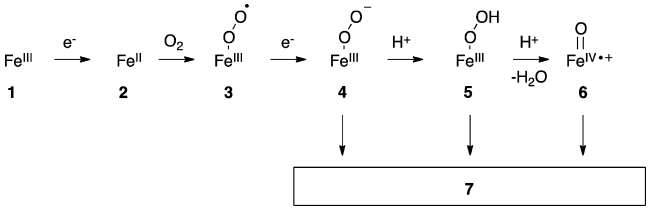


reduction of the ferric heme (**1**) to the ferrous state (**2**) by the reductase domain that originated from NADPH (Scheme 2). Subsequent $O_2$ binding forms a Fe(II)heme−$O_2$ complex (**3**). A second one-electron reduction by $H_4B$ forms the ferric heme-peroxo intermediate (**4**). In step one, this electron is replenished to the $H_4B$ radical by a reaction initiated by NADPH. In the second step of NOS catalysis, when, stoichiometrically, only one electron is required for product formation but two electrons are needed for oxygen activation, the electron is returned to the $H_4B$ radical from the formed Fe(II)−NO complex. Heme species **4** may be converted to product state **7** directly, or it may accept one proton and form the ferric hydroperoxo species (**5**). Species **5** may lead directly to **7**, or it may be additionally protonated and release $H_2O$, yielding compound I (Cpd I, **6**). Cpd I is the most reactive of the three possible active oxy species and, while experimentally difficult to characterize, is presumed to be the most common reactive species in heme-monooxygenation reactions.[16]

The increased stability of ferrous gsNOS−$O_2$ in comparison with mammalian NOSs has allowed better characterization of NOS heme-oxy intermediates **4** and **5** during catalysis. Cryoreduction/annealing/EPR/ENDOR studies have shown that the ternary ferrous gsNOSoxygenase domain ($gsNOS_{oxy}$)−$O_2$−substrate complex that has been reduced radiolytically by one additional electron at 77 K (in the absence of $H_4B$) is competent to catalyze the first and second steps of the reaction during annealing.[17,18] Detailed EPR/ENDOR analysis of the intermediates arising during annealing of the cryoreduced ternary ferrous $gsNOS_{oxy}$−$O_2$−substrate complex showed that oxidation of L-arginine to NHA is catalyzed by Cpd I, whereas the ferric peroxo/hydroperoxo species (**4**/**5**) participates in the conversion of NHA into HNO and L-citrulline (in the absence of $H_4B$). The low concentration of the hydroperoxy species (**5**) that accumulates during the second stage impedes more detailed characterization of its properties and its contribution to the conversion of NHA into nitric oxide and L-citrulline. Indeed, an unusually large rhombicity of the EPR signal of the detected hydroperoxy species may also be interpreted in terms of a tetrahedral intermediate formed from a nucleophilic addition of ferric peroxo intermediate **4** to a guanidinium oxime. Importantly, these studies also show that the nature of the substrates determines the catalytically active state (Scheme 2): Cpd I (**6**) for L-Arg and peroxo/hydroperoxo ferric intermediate (**4**/**5**) in the case of NHA.[17−19]

Recently, we determined substrate/inhibitor characteristics of methylated analogues of NHA with mammalian NOSs (Figure 1).[20,21] Singly methylated NHAs $N^{\omega}$-methoxy-L-arginine (NMOA) and $N^{\omega}$-hydroxy-$N^{\omega}$-methyl-L-arginine (NHMA) were found to be NO- and citrulline-producing NOS substrates. However, there was a 10−15-fold decrease in $k_{cat}$ for all methylated analogues of NHA and a strong increase in the uncoupling of NO production. $N^{\omega}$-Methoxy-$N^{\omega}$-methyl-L-arginine (NMMA), an analogue in which both the $N^{\omega}$-H proton and the $N^{\omega}$-OH proton are replaced with a methyl substituent, is not a viable NOS substrate, but it fits in the NOS active site well with micromolar binding affinity.[20] These studies did not determine to what extent these changes were the result of a lower intrinsic reactivity of the analogues, as opposed to substrate-induced changes in the heme pocket that led to the generation of alternative active heme species with lower reactivity. In favor of this latter possibility, it was

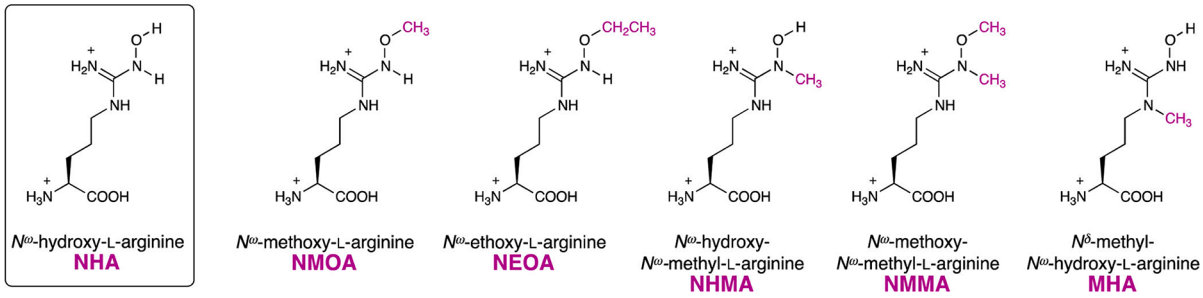


**Figure 1.** NHA substrate analogues.


dx.doi.org/10.1021/bi500485z | *Biochemistry* 2014, 53, 6511−6519

previously shown that the structure of the guanidino moiety can significantly affect the hydrogen-bonding network near the heme active site, which subsequently controls proton transfer events in NOS and tunes its oxidative chemistry.[20,22]

We here report kinetic studies to determine the effects of $N^{\omega}$-methylation of NHA on $H_2O_2$-dependent, gsNOS-catalyzed conversion of substrate to product, comparing results for NHA itself to those for alternative $N^{\omega}$-methylated-NHA substrates, NMOA and NHMA, and inhibitor NMMA. To elucidate the effect of methylating $N^{\omega}$-hydroxy L-arginine on the properties and reactivity of the one-electron-reduced oxy-heme center of gsNOS, we have applied cryoreduction/annealing/EPR/ENDOR techniques, along with measurements of solvent kinetic isotope effects (sKIE), during 160 K cryoannealing of species formed by cryoreduction.[23]

These experiments confirm that step two of gsNOS catalysis involves conformers of $gsNOS_{oxy}$–$O_2$–substrate ternary complexes that generate the peroxoferric state **4** upon 77 K cryoreduction; this state converts during annealing to the catalytically active hydroperoxoferric state **5**. They further reveal that methylation of the guanidinium $N^{\omega}$-H and $N^{\omega}$-OH of NHA inhibits the second, NO-producing, reaction step (Scheme 1) by favoring substates of oxy-gsNOS in which the prompt protonation of **4** formed during 77 K cryoreduction generates an ensemble of unreactive ferric hydroperoxo intermediates, **5**. It is proposed that methylated NHA analogues produce this effect by modifying the hydrogen-bonding network in the distal side of the active site. This mechanism is supported by a quantitative correlation between the yield of the peroxo ferric intermediate trapped at 77 K and the yield of L-citrulline formed by reaction of the hydroperoxo ferric intermediate during annealing of the cryoreduced samples. The present results again show how variations in the properties of the substrate can modulate the reactivity of a monooxygenase;[17,18,24] in this case, methylation of the guanidinium moiety both finely controls the proton transfer events in NOS and tunes the oxidative chemistry of the hydroperoxoferriheme.

## MATERIALS AND METHODS

**Materials.** All chemicals, unless otherwise noted, were obtained from Sigma-Aldrich and used without further purification.

**Protein Purification.** $gsNOS_{oxy}$ was expressed and purified as previously described;[11] iNOS was expressed and purified as described.[20]

**Substrate Synthesis.** Substrate analogues NMOA, NHMA, NMMA, and MHA (Figure 1) were synthesized as previously described.[20]

**Determination of Binding Constants of NHA and Its Analogues to gsNOS.** The determination of binding affinities of NHA and its methylated analogues for $gsNOS_{oxy}$($K_s$) was performed spectrophotometrically as described previously[20,25] and is based on conversion of the low-spin complex of ferric $gsNOS_{oxy}$ with imidazole (ImH) into the high-spin state in the presence of the analogues, induced by the competitive displacement of ImH coordinated to heme iron(III) during substrate binding. $K_s$ values of analogues were determined using the following equation

$$\text{measured } K_s = \text{actual } K_s(1 + [\text{imidazole}]/K_s \text{ imidazole})$$

where $K_s$ for imidazole was found to be 450 $\mu$M.

**Kinetic Characterization of Substrate Oxidation with $H_2O_2$.** $H_2O_2$-dependent nitrite formation was measured for each substrate with $gsNOS_{oxy}$ and murine iNOS in 96-well microplates at 25 °C. With a total volume of 100 $\mu$L, each well contained the following: 20 $\mu$M $gsNOS_{oxy}$ or 1 $\mu$M iNOS with 1 mM substrate (arginine, NHA, NMOA, or NHMA), 10 $\mu$M $H_4B$, and 20 mM $H_2O_2$ in 50 mM Tris buffer, pH 7.8, 10% glycerol, 150 mM NaCl. The reaction was stopped at various time points by adding Griess reagent (50 $\mu$L of each G1 and G2).[26] Product formation was monitored by measuring the absorbance at 540 nm. Nitrite produced was quantified on the basis of nitrate standards. Reported $k_{obs}$ (observed rate) values represent averages from at least three experiments.

**LC–MS Analysis of Reaction Products after Cryoreduction and Annealing.** Urea (6 M final) was added to dislodge products from the enzyme. Samples were filtered through 10 kDa MW cutoff filters (Millipore) to remove $gsNOS_{oxy}$. Amino acids in the flow through were then NDA-derivatized as described[27] and separated by reversed-phase liquid chromatography–mass spectrometry using an Agilent 1200 series purification system equipped with a diode array detector (SL 1315C) set to 460 and 254 nm and an Agilent 6130A Single Quad detector using atmospheric pressure electrospray ionization (API-ES) in the positive mode. A Phenomenex Gemini-NX C18 (4.6 × 50 mm, 5 $\mu$m, 100 Å) column was used with solvent A as LC–MS grade water + 0.1% formic acid and solvent B as LC–MS grade ACN + 0.1% formic acid. A gradient from 10% B to 90% B over 10 min was used at 1 mL/min. NDA–amino acid conjugates were found to have the following retention times: NDA–NHA, 4.2 min; NDA–citrulline, 6.2 min; NDA–NMOA, 4.4 min; NDA–NHMA, 4.4 min; and NDA–NMMA, 4.6 min. On the basis of standard samples, substrates and L-citrulline were found to ionize at approximately the same ratio and therefore percent turnover was determined from integration of the MS peak areas.

**Sample Preparation for Cryoreduction.** The samples of ternary $gsNOS_{oxy}$–$O_2$–substrate complexes for cryoreduction were prepared as described previously.[18] Typically, the samples contained 500 $\mu$M $gsNOS_{oxy}$ and 1.5 mM substrate in a 1:1 (v/v) mixture of 0.1 M Tris buffer, pH 8.3, 150 mM NaCl/ethylene glycol. In the samples prepared in $D_2O$/ethylene glycol-$d_2$, the pH was adjusted to 7.9 (as measured by a pH electrode), which is equivalent to pH 8.3 in $H_2O$/ethylene glycol mixture.[28] $\gamma$-Irradiation of the frozen hemoprotein solution at 77 K was performed for ~15 h (dose rate, 0.15 Mhrad/h; total dose, 2.3 Mr) using a Gammacell 220 $^{60}$Co.

Aqueous Tris buffer is known to show a larger temperature variation than potassium phosphate (KPi) buffer, but this behavior is modified in the presence of high glycerol concentrations. As a result, we used optical spectroscopic examination of the metMb aquo/hydroxo equilibrium at 77 K, metMb($H_2O$) (high spin) = MetMb($OH^-$) (low-spin) + $H^+$, to compare the effect of temperature on the Tris/glycerol buffer system employed with that of KPi/glycerol buffer. Optical absorbance spectra at 77 K were acquired from samples in EPR tubes in a quartz finger Dewar flask with an Ocean Optics USB2000 spectrophotometer.

We find that the apparent p$K_a$ of the metMb aquo/hydroxo transition determined spectrophotometrically for 50% glycerol/0.2 M buffer at 77 K with phosphate and Tris buffers are 8.2 and 7.5, respectively (pH values measured at ambient). This finding implies that the pH of the frozen Tris/glycerol buffer solution is ~0.7 units higher than that measured in phosphate buffer. This implies that the cryoreduction experiments carried


dx.doi.org/10.1021/bi500485z | Biochemistry 2014, 53, 6511–6519

out with Tris/glycerol buffer solutions made up to pH = 8.3 correspond to pH ∼ 9 in the frozen solution.

Multiple lines of evidence have long established that cryoreduction at the dose used here has negligible effect on hemeprotein structure and enzymatic activity.[23] In the present study, the clearest demonstration that this is the case is the observation of quantitative formation of product for cryoreduced gsNOS with NHA and NMA substrates. For completeness, enzymatic activities were measured in fluid solution at ambient temperatures with procedures described above (addition of Griess reagent, etc.) before and after freezing, irradiation, and annealing. The activities of gsNOS before and after this cryoreduction procedure are identical within experimental error (±10%). Finally, subsequent to cryoreduction/annealing, all samples were reduced with dithionite and treated with CO, and the absorptivities compared with those before irradiation; in no case was the absorptivity decreased by more than 5%.

Annealing over a temperature range of 77−270 K was performed by placing the EPR sample in the appropriate bath (*n*-pentane or methanol cooled with liquid nitrogen) and then refreezing in liquid nitrogen.

**EPR Spectroscopy.** X-band CW EPR spectra were recorded on a Bruker ESP 300 spectrometer equipped with an Oxford Instrument ESR 910 continuous He flow cryostat. Most EPR spectra were collected at 28 K at 9.63 GHz, with a modulation amplitude of 10 G, modulation frequency of 100 kHz, sweep time of 140 s, and time constant of 82 ms. $\gamma$-Irradiation at 77 K yields an intense EPR signal at g = 2 from radiolytically generated radicals; such signals were truncated in the reported spectra for clarity. In addition, $\gamma$-irradiation produces hydrogen atoms within the fused silica tubes, and these give a characteristic hyperfine doublet with $A(^1H) \approx 507$ G. Upon annealing at temperatures above 77 K, both radical and H atom signals decrease.

Kinetic progress curves of intermediates during cryoannealing were obtained by fitting populations derived from EPR spectra collected during stepwise annealing at fixed temperature to eqs 1 and 2 (below). Populations of the intermediates as a function of annealing times were determined by simulating the experimental EPR spectra in the low-spin ferriheme region as a sum of individual contributions from the three interconverting low-spin intermediates, **4**, **5**, and **2.47**, using the Bruker Symphonia program. As there is no increase in high-spin signal during annealing, the sum of these three is constant, and the fractional population of an intermediate is determined as the ratio of the double integration of its simulated EPR signal to the total double integral of the three contributors. We estimate the errors in the resulting fractional populations to be less than ±10%. The populations as a function of annealing time were fit to the kinetic scheme of eq 1 (below) assuming stretched-exponential kinetics, as embodied in eq 2, using Mathcad.[29]

## RESULTS AND DISCUSSION

**Binding Constants of NHA Analogues for Ferric gsNOS.** Binding affinities ($K_s$) of the methylated substrate analogues with ferric $gsNOS_{oxy}$ were determined using the spectroscopic binding assay described in the Materials and Methods and are presented in Table 1. Methylation of NHA results in a significant decrease in the binding affinity for gsNOS (Table 1). The binding affinities of the methylated analogues depend on the methylation position and decrease in the order NMMA > NHMA> NMOA> MHA (Table 1).

**Table 1. Binding Affinities ($K_s$) for NHA Analogues with $gsNOS_{oxy}$ and with iNOS**

| | $K_s$ ($\mu$M) | |
|---|---|---|
| | gsNOS | iNOS |
| NHA | 1.5 ± 0.4 | 29 ± 4 |
| NMOA | 29 ± 2.2 | 122 ± 20 |
| NHMA | 17 ± 3.5 | 34 ± 4 |
| NMMA | 12 ± 1.5 | 70 ± 5 |
| MHA | >10 mM | >10 mM |

Interestingly, all NHA analogues have a higher binding affinity for $gsNOS_{oxy}$ than for mammalian iNOS (Table 1), although the relative order of binding affinities of the analogues for $gsNOS_{oxy}$ and iNOS is nearly conserved.

Complexes of NHA, NMOA, NHMA, and NMMA with ferric gsNOS, like substrate-free $gsNOS_{oxy}$, show EPR spectra (Figure S1) characteristic of high-spin pentacoordinated ferriheme. As shown in Table 2, methylation of the guanidinium moiety of NHA results in relatively small shifts of **g**-tensor components of the high-spin ferriheme center. This observation suggests that the substrate modifications do not induce significant changes of the Fe(III)−S(Cys) bond strength relative to NHA binding and do not sterically perturb the heme conformation and its environment. This conclusion is consistent with recently reported X-ray data for complexes of these methylated NHA analogues with the ferric nNOS oxygenase domain.[20] Unlike the methylated analogues of NHA considered above, MHA has the poorest affinity for $gsNOS_{oxy}$ and forms a low-spin complex with the oxidized enzyme whose rhombic EPR signal, **g** = [2.43, 2.29, 1.914] (Figure S1 and Table 2), is similar to that of *N*-alkyl- and *N*-aryl-*N*′ hydroxyguanidines complexed with mammalian NOSs, in which the guanidine N-OH group is coordinated to ferric heme.[30] The crystal structure of the NOS−MHA complex shows that the presence of an $N^{\delta}$-methyl destroys the planarity of guanidine, resulting in shortening of the distance between the $N^{\omega}$-hydroxyl group and the heme iron(III) that favors the formation of a coordination bond.[20]

**Table 2. g-Tensor Components for Ferric $gsNOS_{oxy}$ and Its Complexes with NHA and the Methylated NHA Derivatives**

| | | $g_{max(x)}$ | $g_{mid(y)}$ | $g_{min(z)}$ |
|---|---|---|---|---|
| no substrate | HS | 7.70 | 4.07 | 1.80 |
| | LS | 2.42 | 2.28 | 1.92 |
| NHA | HS | 7.85 | 3.92 | 1.77 |
| NMOA | HS | 7.69 | 4.08 | 1.80 |
| NHMA | HS | 7.73 | 4.05 | 1.80 |
| NMMA | HS | 7.80 | 4.02 | 1.80 |
| MHA | HS | 7.745 | 4.09 | 1.80 |
| | LS (major) | 2.43 | 2.29 | 1.914 |

**Activity of gsNOS with Methylated NHA Analogues.** gsNOS does not have a reductase domain associated with it that would require an exogenous source of electrons for dioxygen activation. $H_2O_2$ was previously shown to serve as cosubstrate in $gsNOS_{oxy}$-catalyzed L-arginine and NHA turnover.[31] Therefore, the activity of $gsNOS_{oxy}$ with NHA analogues was estimated from the rate of nitrite production in the presence of $H_2O_2$. Nitrite was quantitated using the Griess reagent at various time points.[25] Product formation was linear with time, allowing for determination of an observed


dx.doi.org/10.1021/bi500485z | *Biochemistry* 2014, 53, 6511−6519

initial rate, which we have termed $k_{obs}$. Data from the kinetic measurements are presented in Table 3. gsNOS shows high

**Table 3. $k_{obs}$ for Substrate Analogues and $H_2O_2$-Dependent gsNOS and iNOS Catalysis**

| | $k_{obs}$ (nmol $NO_2^-$/nmol NOS/h) | |
|---|---|---|
| | gsNOS | iNOS |
| L-arginine | 3.5 ± 0.6 | 0.07 ± 0.05 |
| NHA | 7.1 ± 1.6 | 3.0 ± 0.9 |
| NMOA | 1.3 ± 0.6 | [a] |
| NHMA | 3.7 ± 1.1 | [a] |
| NMMA | 0.1 ± 0.1 | 0.1 ± 0.05 |

[a]No $NO_2$ produced.

activity with L-arginine and NHA (Table 3). Substitution of the $N^{\omega}$-H (NHMA) and $N^{\omega}$-OH (NMOA) protons of NHA with methyl groups results in 2- and 5-fold decreases, respectively, in substrate activity; replacing both protons (NMMA) abolishes all reactivity (Table 3). For comparison, activities of mammalian iNOS with NHA analogues in the presence of $H_2O_2$ were also measured, but in this case, only NHA was found to produce a detectable level of nitrite. Interestingly, we show here that L-arginine is a poor substrate for $H_2O_2$-dependent catalysis by iNOS, similar to a finding by Marletta and co-workers for eNOS,[32] whereas it is a good substrate for gsNOS.

The inactivity of peroxide-shunt pathways in the first half-reaction of mammalian NOS (Scheme 1) can be explained either by suppression of the binding of $H_2O_2$ to the heme iron(III) in the presence of bound L-arginine (e.g., L-arginine can sterically impede coordination of $H_2O_2$ to heme iron(III), as it does to the binding of water) or by poor proton donation from the L-arginine guanidinium group to the heme-coordinated $H_2O_2$ caused by an unfavorable geometry of $N^{\omega}$-$H_2^+$/Fe(III)-OOH. The latter explanation is supported by the fact that the primary product of cryoreduction of mammalian eNOS−$O_2$−L-Arg trapped at 77 K is the peroxy ferric intermediate (**4**), in contrast to the trapping of the hydroperoxo intermediate (**5**) in ferrous $gsNOS_{oxy}$−$O_2$−L-Arg.[17,18] Suppression of proton delivery is expected both to slow the rate of generation of CpdI and, as predicted by DFT computations, to lower the reactivity of protonated L-arginine substrate as compared to deprotonated L-arginine with ferrylheme.[33] In this interpretation, the difference in efficacy of the peroxide shunt reaction for gsNOS and mammalian NOSs indicates the presence of structural differences in the oxyheme environments in the presence of L-arginine, in particular, differences of the proton delivery network coupled to the distal oxygen of the peroxo ligand in the cryogenerated peroxo intermediate. These structural distinctions might be responsible for the different effects from methylation of $N^{\omega}$-OH and $N^{\omega}$-H on peroxide shunt activities of gsNOS and iNOS (sensitivities of $H_2O_2$-dependent activities of gsNOS and iNOS to $N^{\omega}$-OH and $N^{\omega}$-H replacement by a methyl group) (Table 3).

**EPR of Cryoreduced Ternary $gsNOS_{oxy}/O_2/N^{\omega}$-Methylated NHA Complexes.** EPR spectra of radiolytically reduced ternary ferrous $gsNOS_{oxy}$−$O_2$ complexes with NHA and its methylated analogues at 77 K are presented in Figure 2. The spectrum of the cryoreduced oxy−$gsNOS_{oxy}$−NHA complex shows a dominant rhombic EPR signal with **g** = [2.27, 2.17, nd]. This signal was shown previously to belong to the cryogenerated peroxo-ferriheme (**4**) species denoted as the **g**

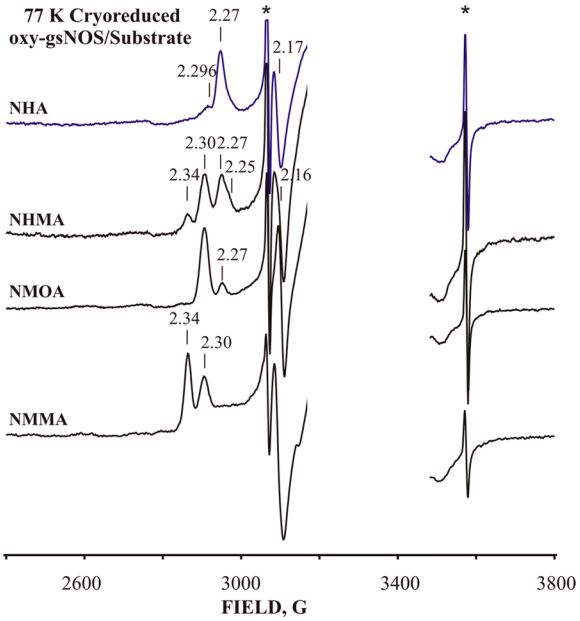


**Figure 2.** X-band CW EPR spectra of cryoreduced ternary complexes oxy gsNOS with NHA, NHMA, NMOA, and NMMA. The H atom doublet signal is marked by an asterisk. Instrument conditions: $T$ = 28 K; modulation amplitude, 10 G; microwave power, 10 mW, microwave frequency, 9.364 GHz.

**2.27** species.[18] Methylation of $N^{\omega}$-H in NHA results in ∼2-fold decrease of the **g 2.27** signal and appearance of two new rhombic EPR signals, with **g** = [2.303, 2.16, nd] (**g 2.30** species) and **g** = [2.337, 2.16, nd] (**g 2.34** species). Such **g** tensors were previously shown to be characteristic of hydroperoxo ferriheme (**5**) states.[18] The EPR spectrum of the cryoreduced complex with NMOA (Figure 1) is dominated by the **g 2.30** species, with none of the **g 2.34** species and little of the **g 2.27** signal (NMOA suppresses the accumulation of the **g 2.27** species by 10-fold). The EPR spectrum of cryoreduced complex of $gsNOS_{oxy}$−$O_2$ with NMMA shows no **g 2.27** signal; the **g 2.34** signal is dominant, with a strong minority **g 2.30** contribution. Comparative analysis of the EPR spectra shows that the distribution of the cryogenerated hydroperoxy **g 2.30** and **g 2.34** species is affected significantly by the position of the $CH_3$ substituent in guanidine group of NHA (Figure 2).

As proposed previously, cryogenerated **4**/NHA remains unprotonated at 77 K because there is not an appropriately positioned water molecule in the H-bonding network near the distal oxygen of the cryogenerated peroxy ligand that can mediate its protonation at, and even below, 77 K.[18] Accumulation of intermediate **5** during radiolytic reduction at 77 K in the presence of the methylated NHA analogues, rather than intermediate **4**, indicates that binding of these NHA analogues alters the proton-delivery network, presumably introducing a water molecule that facilitates proton delivery to the cryogenerated peroxo ligand of **4** at 77 K. The presence of the two distinct **g 2.30** and **g 2.34** species in cryoreduced ternary complexes of $gsNOS_{oxy}$−$O_2$ with methylated NHA analogues further indicates that a hydrogen bond and/or steric interactions with the bound $O_2$ of the oxy-heme in the presence of the NHA analogues stabilizes the $O_2$ in at least two different conformations.

**Annealing of the Cryoreduced Ternary $gsNOS_{oxy}$−$O_2$−Substrate Intermediates.** As shown previously, the 77 K


dx.doi.org/10.1021/bi500485z | Biochemistry 2014, 53, 6511−6519

cryogenerated peroxy gsNOS−NHA complex (**4**/NHA) is competent to quantitatively convert bound substrate into citrulline and HNO during cryoannealing.[18] Kinetic studies further suggested that **4**/NHA converts to the hydroperoxo ferriheme species, **5**/NHA, during cryoannealing and that this state is catalytically active in the conversion of NHA into product;[18] more detailed kinetic studies presented here support that conclusion.

As shown in Figure 3, progressive annealing of cryogenerated **4**/NHA at 160 K causes its EPR signal to decay, and early in this process a weak signal appears with $g_1$ = **2.36**, which is assigned to the catalytically active hydroperoxo ferric species **5**/NHA. Further annealing produces two low-spin ferriheme EPR signals associated with conformers of the primary product of NHA hydroxylation, one with **g** = [2.47, 226; 1.91] (major, denoted as **g 2.47** state) and the other with **g** = [2.49, 2.226, 191] (minor) (Figure 3).[18] As described previously, the **g 2.47** state shows a strongly coupled $^1$H ENDOR signal that is exchangeable in $D_2O$, with $A_{max}$ ~10 MHz, comparable with the $^1$H ENDOR signal from the water of low-spin aqua ($H_xO$, $x$ = 1 or 2) ferric NOS,[18] indicating that this product state contains an aqua-ferriheme, as expected for reaction of **5** with NHA substrate. The small differences in the **g**-values of the **g 2.47** product state and the resting aqua-ferriheme state likely reflect the perturbing effect of the products that temporarily reside in the heme pocket. The **g 2.47** signal disappears at temperatures above 170 K, and its decay is accompanied by the appearance of an EPR signal of the NO-ferroheme, **g** = [2.08, nd, 1.969] (Figure 3). These results imply that annealing of cryogenerated **4**/NHA at 160−170 K converts it to the **g 2.47** ferriheme, generating L-citrulline and HNO/$NO^-$ as the primary products of NHA oxidation; during subsequent annealing at $T$ > 170 K, the HNO reacts with the ferriheme to generate the NO-ferroheme adduct.

The above analysis rests on the assignment of the **g 2.36** species as the catalytically active **5**/NHA. However, the low concentration of this **2.36** species precludes its detailed spectroscopic characterization. Thus, although the **g**-values of this species are compatible with the assignment as **5**/NHA, the unusually large rhombicity of the EPR signal of the **2.36** intermediate might instead be interpreted in terms of an Fe−O−O−C tetrahedral-carbon intermediate formed from a nucleophilic addition of the peroxo moiety of the ferric peroxo intermediate to a guanidiniumoxime. To test the assignment, we extended the cryoannealing studies of **4**/NHA at 160 K by examining not only of the loss of **4**/NHA at 160 K but also the parallel appearance and loss of **g 2.36** and the progressive appearance of **g 2.47**, doing so with both $H_2O$ (Figure 4A) and $D_2O$ (Figure 4B) buffers.

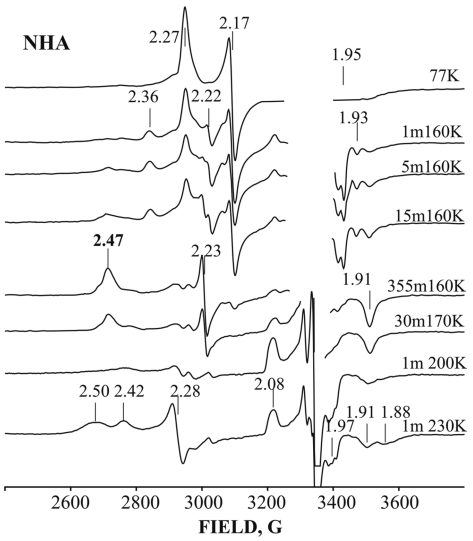


**Figure 3.** Low-spin region of EPR spectra of cryoreduced oxy gsNOS−NHA annealed under the indicated conditions (no changes are observed in high-spin region). Instrument conditions as those in Figure 2.

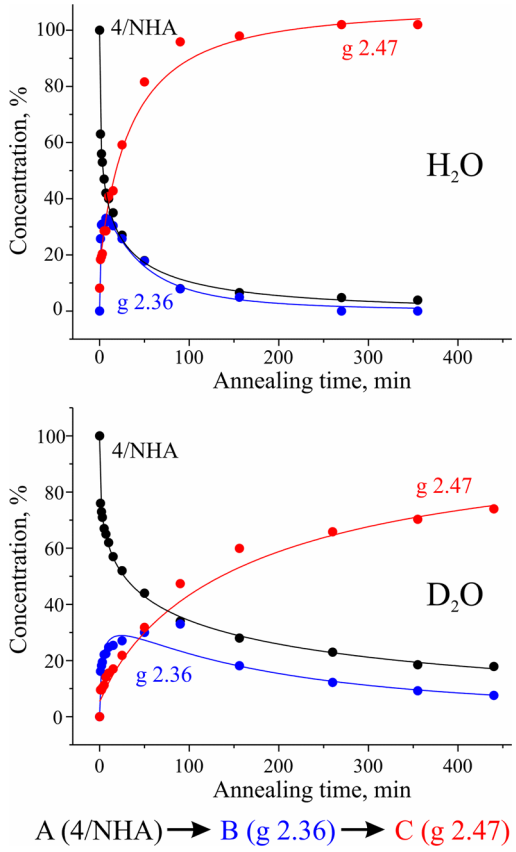


**Figure 4.** Kinetic progress curess for the 160 K cryoannealing of **4**/NHA (A), **5**/NHA = **g 2.36** (B), and **g 2.47** primary product (C). Solid lines are fits to the equation given in the Materials and Methods.

Figure 4A shows that the progress curves for the three species during 160 K cryoannealing can be well-described by the coupled first-order differential equations for a two-step kinetic scheme

$$\mathbf{4}/\text{NHA (A)} \rightarrow \mathbf{g\ 2.36}\ \text{(B)} \rightarrow \mathbf{2.47}\ \text{(C)} \quad (1)$$

in which both of the two successive steps ($i$ = 1, 2) exhibit "stretched exponential" behavior,[27] as seen before for the decay of **4**/NHA.[18] The differential equations for such a kinetic model are given in eq 2, where the rate coefficients decrease in time and are characterized by decay times, $\tau_i$ and coefficients, $a_i$.[34]


dx.doi.org/10.1021/bi500485z | Biochemistry 2014, 53, 6511−6519

$$\frac{dA(t)}{dt} = -k_1(t)A(t)$$

$$\frac{dB(t)}{dt} = k_1(t)A(t) - k_2(t)B(t) \quad k_i(t) = \frac{a_i}{\tau_i}\left(\frac{t}{\tau_i}\right)^{a_i-1}$$

$$A(t) + B(t) + C(t) = 1 \qquad (2)$$

This behavior is indicative that the monitored species exist as a distribution of conformational substates, with the decay constant varying over the distribution. In this formulation, each step is described by an average reaction time, $\tau$, while the breadth of the distribution is reflected in the constant, $0 < a \leq 1$, with smaller values for $a$ corresponding to greater breadth of distribution.

As can be seen in Figure 4, this equation fits the observed time courses in both H and D isotopic buffers very well; the rate parameters are listed in Table 4. Most importantly, the

**Table 4. Kinetic Parameters (Eqs 1 and 2) for Cryoannealing of 4/NHA (Figure 4)**

| | first step | | second step | |
|---|---|---|---|---|
| | $\tau_1$ | $a_1$ | $\tau_2$ | $a_2$ |
| $H_2O$ | 11 min | 0.36 | 14 min | 0.66 |
| $D_2O$ | 84 min | 0.34 | 50 min | 0.62 |
| sKIE[a] | ~7.5 | | ~3.5 | |

[a] $\tau_i(D_2O)/\tau_1(H_2O)$.

kinetic coupling between **4**/NHA decay and **g 2.36** formation occurs with a strong solvent kinetic isotope effect (sKIE) (Table 4): $sKIE(160\ K)_1 = \tau_1(D_2O)/\tau_1(H_2O) = 84\ min/11\ min \approx 7.5$ (85% $D_2O$), as reported.[18] This confirms that the **g 2.36** species is indeed **5**/NHA formed by protonation of the peroxo moiety in **4**/NHA and is not a product of the reaction of **4**/NHA with substrate, as such a process would not involve proton transfer and a strong sKIE. The subsequent kinetic coupling of **g 2.36** to the formation of the **2.47** product state, combined with the ENDOR evidence that Cpd I is not the reactive species,[18] then confirms that **g 2.36** = **5**/NHA is indeed the reactive species in NHA hydroxylation. The observation of a significant sKIE associated with this process, $\tau_2(D_2O)/\tau_2(H_2O) = 50\ min/14\ min \approx 3.6$ (85% $D_2O$) (Table 4), indicates a difference in the reactivity of the OOH and OOD moieties of **5** and/or of the solvent-exchanged NHA. The conclusion that **5**/NHA is the reactive species in the second step of NO generation by gsNOS correlates well with our findings that gsNOS efficiently catalyzes $H_2O_2$-dependent conversion of NHA into NO and citrulline.

HPLC analysis of the cryoreduced oxy gsNOS/NHA samples further annealed at 273 K shows quantitative conversion of bound NHA to L-citrulline (in our experiments, this corresponds to formation of 0.20 ± 0.02 mM L-citrulline), confirming the catalytic significance of the cryoreduction measurements. As a rule, the amount of the gsNOSFe(II)−NO complex detected in the annealed samples is less than the amount of L-citrulline, but this can be attributed both to an instability of the NO adduct of NOS in the presence of $O_2$ and to side reactions of HNO with $O_2$ and products of radiolysis. Indeed, as follows from the data presented in Figure 3, even changing the temperature of annealing from 200 to 237 K results in a remarkable decrease of the Fe(II)−NO signal.

As shown in Figures 5 and S2−S3, the hydroperoxo ferric intermediates (**5**) that accumulate upon 77 K cryoreduction in

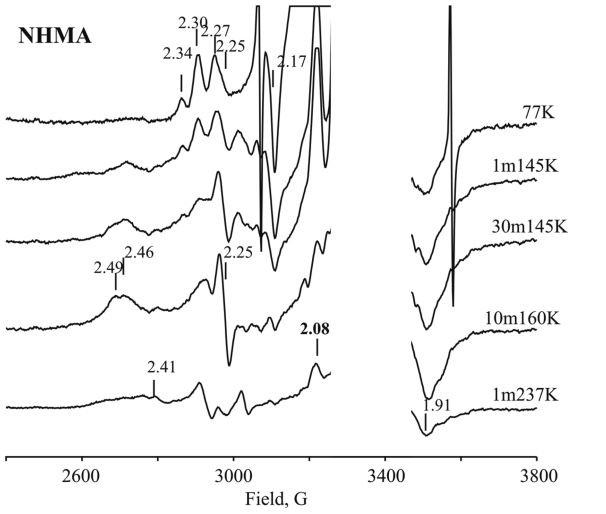


**Figure 5.** EPR spectra of cryoreduced oxy gsNOS−NHMA annealed under the indicated conditions. Instrument conditions are as those in Figure 2. The relative fractional populations of species A−C were determined by reproducing the observed spectrum as a sum of contributions from simulations of the three individual species, as calculated using the Bruker Symphonia program (see Materials and Methods).

the presence of methylated analogues of NHA (Figure 2) decay significantly faster then cryogenerated **4**/NHA; this decay usually is completes by 145 K instead of 160 K, as in the case of NHA. Low-spin ferriheme states with **g** ~ [2.45−2.50, 2.25, 1.90], quite distinguishable from the **g 2.47** product species, are produced by the decays with methylated analogues. During annealing up to 237 K, only weak EPR signals characteristic of Fe(II)−NO are observed in the case of cryoreduced $gsNOS_{oxy}$−NHMA (Figure 5), and no signal from the Fe(II)−NO complex was detected during annealing of the cryoreduced ferrous $gsNOS_{oxy}-O_2$ complexes with NMOA and NMMA (Figures S2−S3). Note that the EPR spectrum of the intermediates formed during cryoannealing of samples with **5**−NHMA, **5**−NMOA, and **5**−NMMA resemble that reported for **5**−L-arginine,[18] which was shown to involve hydroxylation by Cpd I. However, with the analogues, the absence of any FeNO products of reaction in the case of NMOA and NMMA show that low-spin ferriheme states formed during relaxation of **5**−NMOA and **5**−NMMA result not from product formation but most likely from reduction of Cpd I to the aqua ferric state by radiolytically generated radicals, as happens for cryoreduced substrate-free $gsNOS_{oxy}-O_2$.[18]

It is important to note that the **g**-values of the nonreactive ferric hydroperoxo species trapped during 77 K cryoreduction of the oxy gsNOS/methylated NHA analogues (Figure 5) differ from those of the reactive **g 2.36** form of **5**/NHA generated by annealing **4**/NHA. This observation indicates that methylation of NHA alters the structure and lowers the reactivity of this form of the hydroperoxy ferric intermediate with these substrates. It seems likely, in fact, that the nonreactive forms of **5** are diverted to the formation of Cpd I.

The key findings of this study are as follows: (i) Measurements of sKIEs during 160 K cryoanneling of the **g 2.26** peroxo ferric species **4**/NHA state trapped during 77 K


dx.doi.org/10.1021/bi500485z | Biochemistry 2014, 53, 6511−6519

cryoreduction of oxy NOS/NHA confirm the previous conclusion that NHA is hydroxylated by the **g 2.36** hydroperoxo ferriheme state of gsNOS. Product analysis for the cryoreduced samples with NHMA, NMOA, and NMMA annealed at 273 K showed that L-citrulline formation during relaxation of cryoreduced samples of $gsNOS_{oxy}$–$O_2$ with NHA and its methylated analogues is 0.2, 0.13, 0.03, and ~0.01 mM, respectively. These yields of L-citrulline correlate quite well with the intensity of the EPR **g 2.26** signal of peroxo ferric species **4**, which converts to the reactive **g 2.36** form of **5**. There is also some correlation between the yield of L-citrulline in these experiments and the $k_{cat}$ for $H_2O_2$-dependent conversion of the substrates by gsNOS (Table 3). Correspondingly, no detectable amount of cyanoornithine, formed when Cpd I is the reactive species, was found in the samples.[19] (ii) The formation, structure, and reactivity of **5** are modulated by the methylation of NHA.

## CONCLUSIONS

Recently, it has been shown that the replacement of protons of $N^{\omega}$-H and $N^{\omega}$-OH of NHA for $CH_3$ strongly decreases the rate of conversion of NHA to L-citrulline by nNOS and iNOS and causes significant uncoupling.[20] The data presented herein allow more detailed insight into the possible mechanism of the inhibitory effects of the methylated analogues. Catalysis measurements show that $N^{\omega}$-methylation of NHA has a qualitatively similar effect on $H_2O_2$-dependent, gsNOS-catalyzed conversion of substrate to product. The cryoreduction data show that binding $N^{\omega}$-H- and $N^{\omega}$-OH-methylated NHA analogues significantly enhance proton delivery to the distal oxygen of the cryogenerated peroxo ligand at 77 K (likely from NHA itself),[18] thereby decreasing the yield of the peroxo intermediate trapped at 77 K and leading to the observation of the hydroperoxo intermediate at that temperature, as summarized in Table 5. As shown previously, the presence of an ordered water molecule near the distal oxygen of the peroxide ligand is essential to this delivery process; therefore, we conclude that the methylated NHA analogues have induced the binding of such a water molecule to the oxyheme center.[18]

**Table 5. Results of Cryoreduction/Annealing**

| | observed, 77 K | cryoannealing | product |
|---|---|---|---|
| NHA | **4**/NHA | **5**/NHA | + |
| NHMA | **4**/NHMA | **5**/NHMA | + |
| | **5′**/NHMA | **5′**/NHMA | — |
| NMOA | **4′**/NMOA + **5′**/NMOA | **5′**/NMOA | — |
| NMMA | **5′**/NMMA | **5′**/NMMA | — |

Annealing experiments have shown that conformers of $gsNOS_{oxy}$–$O_2$–substrate ternary complexes that generate the peroxoferric state **4** convert to a catalytically active hydroperoxoferric state **5** (Table 5). Methylation of NHA causes a redistribution of the primary products of cryoreduction, increasing the population of conformational substates of the parent $gsNOS_{oxy}$–$O_2$–substrate complex in which intermediate **4** does not accumulate at 77 K but is protonated to form an ensemble of unreactive ferric hydroperoxo intermediates, **5**. Methylation likely produces the redistribution by introducing an ordered water molecule adjacent to the distal oxygen of the Fe–O–O moiety that facilitates delivery of the proton(s) to the one-electron-reduced oxy-heme moiety. The **g**-values of the resultant intermediate **5** differs from those of the reactive **g 2.36** **5**/NHA intermediate, indicating that methylation-induced changes in the structure of **5** likely reduce its reactivity.

These results once again show how variations in the properties of the substrate can modulate the reactivity of a monooxygenase;[17,18,23] in this case, methylation of the guanidinium moiety both finely controls the proton transfer events in NOS and tunes the oxidative chemistry of the hydroperoxoferriheme. The present findings further indicate that the difference in efficacy of the peroxide shunt reaction for gsNOS and mammalian NOSs reflects differences of the proton-delivery network coupled to the distal oxygen of peroxo ligand in the cryogenerated peroxo intermediate in the presence of L-arginine.

## ASSOCIATED CONTENT

### Supporting Information

EPR spectra of ferric gsNOS and complexes with NHA and methylated analogues, EPR spectra of cryoreduced $gsNOS_{oxy}$–NMOA, and EPR spectra of cryoreduced $gsNOS_{oxy}$–NMMA. This material is available free of charge via the Internet at http://pubs.acs.org.

## AUTHOR INFORMATION


### Corresponding Authors

*(B.R.C.) Phone: 607-254-8634; E-mail: bc69@cornell.edu.
*(R.B.S.) Phone: 847-491-5653; Fax: 847-491-7713; E-mail: Agman@chem.northwestern.edu.
*(B.M.H.) Phone: 847-491-3104; E-mail: bmh@northwestern.edu.

### Present Address

‖(K.J.L.) Beloit College, Department of Chemistry, 700 College St, Beloit, Wisconsin 53511, United States.



### Funding

This work was supported by the NIH (HL13531 to B.M.H., GM049725 to R.B.S., and a Ruth L. Kirschstein Postdoctoral Award, GM09184-01, to S.E.C.) and by the NSF (CHE-0749997 to B.R.C.).


### Notes

The authors declare no competing financial interest.

## ACKNOWLEDGMENTS

We thank Prof. Howard Halpern, University of Chicago, for arranging access to the Gammacell 220 Irradiator.

## REFERENCES


(1) Stuehr, D. J., Santolini, J., Wang, Z.-Q., Wei, C.-C., and Adak, S. (2004) Update on mechanism and catalytic regulation in the NO synthases. *J. Biol. Chem. 279*, 36167–36170.

(2) Wei, C.-C., Wang, Z.-Q., Hemann, C., Hille, R., and Stuehr, D. J. (2003) A tetrahydrobiopterin radical forms and then becomes reduced during $N^{\omega}$-hydroxyarginine oxidation by nitric-oxide synthase. *J. Biol. Chem. 278*, 46668–46673.

(3) Stuehr, D. J., Wei, C.-C., Wang, Z., and Hille, R. (2005) Exploring the redox reactions between heme and tetrahydrobiopterin in the nitric oxide synthases. *Dalton Trans.*, 3427–3435.

(4) Brunel, A., Santolini, J., and Dorlet, P. (2012) Electron paramagnetic resonance characterization of tetrahydrobiopterin radical formation in bacterial nitric oxide synthase compared to mammalian nitric oxide synthase. *Biophys. J. 103*, 109–117.

(5) Ignarro, L. J. (2002) Nitric oxide as a unique signaling molecule in the vascular system: a historical overview. *J. Physiol. Pharmacol. 53*, 503–514.

(6) Alderton, W. K., Cooper, C. E., and Knowles, R. G. (2001) Nitric oxide synthases: structure, function and inhibition. *Biochem. J. 357*, 593−615.
(7) Dawson, V. L., and Dawson, T. M. (1998) Nitric oxide in neurodegeneration. *Prog. Brain Res. 118*, 215−229.
(8) Vallance, P. P., and Leiper, J. J. (2002) Blocking NO synthesis: how, where and why? *Nat. Rev. Drug Discovery 1*, 939−950.
(9) Nakamura, T., and Lipton, S. A. (2008) Emerging roles of S-nitrosylation in protein misfolding and neurodegenerative diseases. *Antioxid. Redox Signal. 10*, 87−101.
(10) Chung, K. K. K., and David, K. K. (2010) Emerging roles of nitric oxide in neurodegeneration. *Nitric Oxide 22*, 290−295.
(11) Sudhamsu, J., and Crane, B. R. (2006) Structure and reactivity of a thermostable prokaryotic nitric-oxide synthase that forms a long-lived oxy-heme complex. *J. Biol. Chem. 281*, 9623−9632.
(12) Crane, B. R., Sudhamsu, J., and Patel, B. A. (2010) Bacterial nitric oxide synthases. *Annu. Rev. Biochem. 79*, 445−470.
(13) Wang, Z. Q., Lawson, R. J., Buddha, M. R., Wei, C. C., Crane, B. R., Munro, A. W., and Stuehr, D. J. (2007) Bacterial flavodoxins support nitric oxide production by *Bacillus subtilis* nitric-oxide synthase. *J. Biol. Chem. 282*, 2196−2202.
(14) Agapie, T., Suseno, S., Woodward, J. J., Stall, S., Britt, R. D., and Marletta, M. A. (2009) NO formation by catalytically self-sufficient bacterial nitric oxide synthase from *Sorangium cellulosum*. *Proc. Natl. Acad. Sci. U.S.A. 106*, 16221−16226.
(15) Pant, K., and Crane, B. R. (2006) Nitrosyl-heme structures of *Bacillus Subtilis* nitric oxide synthase have implications for understanding substrate oxidation. *Biochemistry 45*, 2537−2544.
(16) Rittle, J., and Green, M. T. (2010) Cytochrome P450 compound I: capture, characterization, and C−H bond activation kinetics. *Science 330*, 933−937.
(17) Davydov, R., Ledbetter-Rogers, A. A., Martásek, P., Larukhin, M. M., Sono, M. M., Dawson, J. H., Masters, B. S. S., and Hoffman, B. M. (2002) EPR and ENDOR characterization of intermediates in the cryoreduced oxy-nitric oxide synthase heme domain with bound L-arginine or $N^G$-hydroxyarginine. *Biochemistry 41*, 10375−10381.
(18) Davydov, R., Sudhamsu, J., Lees, N. S., Crane, B. R., and Hoffman, B. M. (2009) EPR and ENDOR characterization of the reactive intermediates in the generation of NO by cryoreduced oxy-nitric oxide synthase from *Geobacillus stearothermophilus*. *J. Am. Chem. Soc. 131*, 14493−14507.
(19) Woodward, J. J., Chang, M. M., Martin, N. I., and Marletta, M. A. (2009) The second step of the nitric oxide synthase reaction: evidence for ferric-peroxo as the active oxidant. *J. Am. Chem. Soc. 131*, 297−305.
(20) Labby, K. J., Li, H., Roman, L. J., Martásek, P., Poulos, T. L., and Silverman, R. B. (2013) Methylated $N^{\omega}$-hydroxy-L-arginine analogues as mechanistic probes for the second step of the nitric oxide synthase-catalyzed reaction. *Biochemistry 52*, 3062−3073.
(21) Huang, H., Hah, J.-M., and Silverman, R. B. (2001) Mechanism of nitric oxide synthase. Evidence that direct hydrogen atom abstraction from the OH bond of $N^G$-hydroxyarginine is not relevant to the mechanism. *J. Am. Chem. Soc. 123*, 2674−2676.
(22) Giroud, C., Moreau, M. M., Mattioli, T. A., Balland, V., Boucher, J.-L., Xu-Li, Y., Stuehr, D. J., and Santolini, J. (2010) Role of arginine guanidinium moiety in nitric-oxide synthase mechanism of oxygen activation. *J. Biol. Chem. 285*, 7233−7245.
(23) Davydov, R., and Hoffman, B. M. (2011) Active intermediates in heme monooxygenase reactions as revealed by cryoreduction/annealing, EPR/ENDOR studies. *Arch. Biochem. Biophys. 507*, 36−43.
(24) Davydov, R., Perera, R., Jin, S., Yang, T. Y., Brison, T. A., Sone, M., Dawson, J. H., and Hoffman, B. M. (2005) Substrate modulation of the proprerties and reactivity of the oxy-ferrous and hydroperoxo ferric intermediates of cytochrome P450 cam as shown by cryoreduction-EPR/ENDOR spectroscopy. *J. Am. Chem. Soc. 127*, 1403−1413.
(25) Martell, J. D., Li, H., Doukov, T., Martásek, P., Roman, L. J., Soltis, M., Poulos, T. L., and Silverman, R. B. (2010) Heme-coordinating inhibitors of neuronal nitric oxide synthase. Iron−thioether coordination is stabilized by hydrophobic contacts without increased inhibitor potency. *J. Am. Chem. Soc. 132*, 798−806.
(26) Hevel, J. M., and Marletta, M. A. (1994) Nitric-oxide synthase assays. *Methods Enzymol. 233*, 250−258.
(27) Hurshman, A. R., and Marletta, M. A. (2002) Reactions catalyzed by the heme domain of inducible nitric oxide synthase: evidence for the involvement of tetrahydrobiopterin in electron transfer. *Biochemistry 41*, 3439−3456.
(28) Glascoe, P. K., and Long, F. A. (1960) Use of glass electrodes to measure acidities in deuterium oxide. *J. Phys. Chem. 64*, 188−190.
(29) Lukoyanov, D., Barney, B. M., Dean, D. R., Seefeldt, L. C., and Hoffman, B. M. (2007) Connecting nitrogenase intermediates with the kinetic scheme for $N_2$ reduction by the relaxation protocol and identification of the $N_2$ binding state. *Proc. Natl. Acad. Sci. U.S.A. 104*, 1451−1455.
(30) Lefèvre-Groboillot, D., Frapart, Y., Desbois, A., Zimmermann, J.-L., Boucher, J.-L., Gorren, A. C. F., Mayer, B., Stuehr, D. J., and Mansuy, D. (2003) Two modes of binding of N-hydroxyguanidines to NO synthases: first evidence for the formation of iron-N-hydroxyguanidine complexes and key role of tetrahydrobiopterin in determining the binding mode. *Biochemistry 42*, 3858−3867.
(31) Martin, N. I., Woodward, J. J., Winter, M. B., Beeson, W. T., and Marletta, M. A. (2007) Design and synthesis of C5 methylated L-arginine analogues as active site probes for nitric oxide synthase. *J. Am. Chem. Soc. 129*, 12563−12570.
(32) Pufahl, R. A., Wishnok, J. S., and Marletta, M. A. (1995) Hydrogen peroxide-supported oxidation of $N^G$-hydroxy-L-arginine by nitric oxide synthase. *Biochemistry 34*, 1930−1941.
(33) Cho, K.-B., Carvajal, M. A., and Shaik, S. (2009) First half-reaction mechanism of nitric oxide synthase: the role of proton and oxygen coupled electron transfer in the reaction by quantum mechanics/molecular mechanics. *J. Phys. Chem. B 113*, 336−346.
(34) Phillips, J. C. (1996) Stretched exponential relaxation in molecular and electronic glasses. *Rep. Prog. Phys. 59*, 1133−1207.